Inorganic Chemistry

Article

pubs.acs.org/IC

Unraveling the Polymorphism of [(*p*-cymene)Ru(κN-INA)Cl_2] through Dispersion-Corrected DFT and NMR GIPAW Calculations

Davide Presti, Alfonso Pedone,* and Maria Cristina Menziani*

Dipartimento di Scienze Chimiche e Geologiche, Università di Modena e Reggio-Emilia, 183 via G. Campi, I-41125 Modena, Italy

Supporting Information

ABSTRACT: The structural and $^{13}C/^{1}H$ NMR parameters of the four crystal forms (**1*α***, **1·H_2O**, **1*β***, and **1*γ***) of the solid wheel-and-axle (WAA) metal−organic compound [(*p*-cymene)-Ru(κN-INA)Cl_2] have been studied by means of periodic DFT calculations. The quality of the results obtained strongly depends on a correct description of long-range interactions; thus, in the geometry refinement protocol used, the pure DFT functionals need to be coupled with a dispersion-correction term (B3LYP-D2, B3LYP-D*). The solid-state $^{13}C/^{1}H$ NMR δ_{iso} parameters and ^{13}C MAS NMR spectra, calculated by means of the PBE-GIPAW method, agree well with the experimental data for the four crystal forms (mean absolute deviations of the ^{13}C and ^{1}H δ_{iso} data values lie in the ranges 1.3−2.9 and 0.3−1.0 ppm, respectively). In this context, some revisions in the experimental assignment of the $^{13}C/^{1}H$ NMR δ_{iso} parameters of the **1·H_2O**, **1*β***, and **1*γ*** crystal forms can be suggested. The mismatch in the assignment seems to be due to the rotation of the −COOH moiety, which occurs at the **1*α*−1·H_2O** transition and was not considered in the experiments. Finally, the results obtained suggest the presence of two COOH···Cl hydrogen bonds of comparable strength established by the two molecules in the asymmetric unit of the **1*γ*** polymorph, in partial disagreement with previous findings.

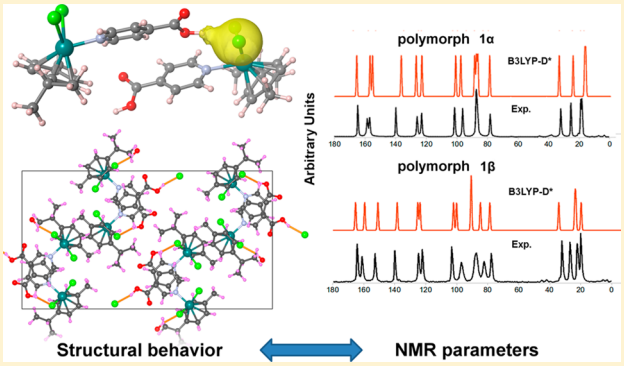

INTRODUCTION

Wheel-and-axle (WAA) compounds represent a class of organic/inorganic molecules characterized by a long, usually linear spacer (axle) and two bulky groups (wheels) at both ends. The shape and the irregularity of these types of structures promote the generation of a widespread supramolecular organization governed by hydrogen bonds and/or dispersive interactions. Therefore, WAAs present well-known host−guest properties and a high tendency to form clathrates with different solvents,[1] thus attracting the interest of many researchers to the design of WAA compounds for applications in heterogeneous catalysis, solid-state "green" chemistry, sensoring, and storage of gases.[2−5]

Very recently, Bacchi and co-workers[2] reported the design of a new series of WAAMOs based on the half-sandwich Ru(II) complex [(*p*-cymene)Ru(κN-INA)Cl_2] (INA = isonicotinic acid) with the aim of obtaining a supramolecular synthon by cyclic supramolecular dimerization of the INA carboxylic groups. The solid [(*p*-cymene)Ru(κN-INA)Cl_2] was obtained in four different crystalline forms: **1*α***, **1·H_2O**, **1*β***, and **1*γ***.

The isolation of the pure metastable **1*γ*** polymorph and its XRPD/NMR characterization were achieved in a subsequent work by the same authors[6] who, in addition, realized that the **1*β*** form is also metastable and, if cooled down slowly, transforms into **1*γ***, not **1*α*** as observed previously. Moreover, some peculiarities in the structure of the **1*β*** polymorph were also reconsidered.[6]

Interestingly, the X-ray single-crystal and powder diffraction, ATR-FTIR, and solid-state NMR (ssNMR) spectroscopic characterization revealed that the main intermolecular interactions governing the supramolecular architecture of **1*α***, **1*β***, and **1*γ*** was not the expected cyclic supramolecular dimer involving the −COOH functions but rather the hydrogen bonds between the chloride ligands (acceptor) bonded to Ru(II) and the carboxylic OH moiety (donor). Moreover, for the **1·H_2O** form the cyclic supramolecular dimerization of the COOH groups of INA is prevented by the inclusion of water.

All of these observations give an idea of the complexity of the [(*p*-cymene)Ru(κN-INA)Cl_2] polymorphism, knowledge of which represents an important challenge, since it implies the characterization of the weak noncovalent interactions determining one molecular packing with respect to the others.

NMR crystallography, that is, the combination of solid-state NMR spectroscopic data with X-ray powder diffraction (XRPD) methods, is a powerful tool to investigate the structure of materials difficult to obtain as large single crystals.[7]

However, the assignment of the observed ^{13}C and ^{1}H solid-state NMR resonances to the atoms belonging to distinct molecules in the asymmetric unit cell is a considerable challenge that can only be met by the help of computational NMR. The successful prediction of chemical shifts and

Received: March 23, 2014
Published: July 14, 2014

quadrupolar coupling constants of various inorganic crystalline and amorphous solids[8−14] as well as of organic molecular crystals and biomolecules[8,15,16] has been achieved by means of recent developments of the gauge including projector augmented wave (GIPAW) method. GIPAW is especially devised for the computation of NMR parameters in extended solids described within periodic boundary conditions, plane wave basis sets, and density functional theory (DFT-GIPAW).[17,18]

The accuracy of the NMR calculation results is strongly dependent on the quality of the structural coordinates employed.[19] Cost-effective energy minimization approaches based on density functional theory can be employed to generate refined structures[20−23] to achieve the best agreement between experimentally measured and ab initio calculated chemical shift tensor components. However, the most common exchange-correlation functionals, based on semilocal electron correlation, do not accurately describe the effects of the dispersive forces, which govern the packing arrangements and the stability of molecular solids. Thus, London-type pairwise corrections based on either empirical[24,25] or nonempirical[26−30] parameters or nonlocal DFT functionals[31−33] must be applied.[34,35]

In this paper, the solid-state $^{13}C/^{1}H$ NMR δ_{iso} parameters and ^{13}C MAS NMR spectra of the **1α**, **1·H$_2$O**, **1β**, and **1γ** crystal forms of [(*p*-cymene)Ru(κN-INA)Cl$_2$] will be calculated by means of the PBE-GIPAW method and the results will be compared with the experimental data. The importance of the quality of the structural coordinates used (i.e., the correct treatment of dispersion interactions in the refinement of the crystal structure of the crystal forms) will be discussed.

COMPUTATIONAL PARAMETERS

Geometry Optimizations. Gaussian-basis DFT calculations were carried out by using a parallel version of the CRYSTAL09 package,[36,37] imposing periodic boundary conditions (PBC). The starting geometries of the **1α** and **1·H$_2$O** crystal forms were taken from ref 2, whereas those of the **1β** and **1γ** crystal forms correspond to the nonrefined geometries of ref 6.

Full geometry optimizations (lattice parameters and atomic displacements) of the **1α**, **1·H$_2$O**, **1β**, and **1γ** crystal forms were performed by using the hybrid B3LYP functional,[38,39] its combination with the "classical" Grimme dispersion correction (B3LYP-D2),[24] and the alternative reparametrization of the Grimme D2 term devised for crystals (B3LYP-D*).[40] Moreover, for the **1β** and **1γ** crystal forms B3LYP-D* geometry optimizations with allowance for the relaxation of the positions of the hydrogen atoms only were also carried out.

The basis set chosen furnishes an optimal characterization of the electronic configuration of the Ru(II) metal−organic synthons and their arrangement within a manifold crystalline framework. Chlorine and ruthenium atoms were described by modified fully relativistic pseudopotentials on core electrons (MDF28 ECP for Ru,[41] SDF10 ECP for Cl[42]—primitive Gaussians with exponents lower than 0.06 have been excluded to avoid basis set linear dependence), and associated double-ζ quality basis sets on valence electrons, taken from the Stuttgart pseudopotential library.[43]

The 6-31G(d) basis set was used for H, C, N, and O atoms; a p-type polarization was added on H atoms and sp-type diffuse functions (consistent with the 6-31+G(d) basis set) were used for N and O atoms. The use of diffuse functions is justified by the fact that N atoms are directly involved in the Ru(II) complex, whereas O atoms can form, depending on the case, the hydrogen bond.

The Monkhorst−Pack grid of *k* points was generated with a shrinking factor of 2 (keyword SHRINK 2 2), that corresponds to 8 *k* points inside the Irreducible Brillouin Zone (IBZ), whereas the DFT integration grid consisted of 75 radial and 974 angular points. The thresholds for Coulomb and exchange series accuracy (keyword TOLINTEG; see ref 35) were set to 10^{-8}, 10^{-8}, 10^{-8}, 10^{-10}, and 10^{-25}.

NMR Calculations. Calculations of NMR parameters were carried out on the crystal structures previously optimized at the B3LYP, B3LYP-D2, and B3LYP-D* level of theory.

The ^{1}H and ^{13}C shielding tensors were computed by means of the gauge including projection augmented wave (GIPAW) approach[44,45] encoded in the CASTEP software[46,47] which uses plane waves as the basis set and the pseudopotential approach to describe the core−valence interactions. All calculations were performed using the PBE exchange-correlation functional[48] without including dispersion-correction terms. In fact, being a posteriori empirical corrections to the DFT energy and forces, they do not directly affect the computation of the NMR parameters. Ultrasoft pseudopotentials included in the CASTEP library were used, and the plane wave basis set was cut at 610 eV. A Monkhorst−Pack grid of minimum sample spacing of 0.04 Å^{-1} in the reciprocal lattice was adopted.

In order to compare the isotropic shielding directly with experimentally measured isotropic chemical shifts, the following relations were used for ^{13}C and ^{1}H, respectively:

$$\delta_{iso}(^{13}C) = -0.960\sigma_{iso} + 166.6$$

$$\delta_{iso}(^{1}H) = -0.944\sigma_{iso} + 29.6$$

which were fitted on the measured isotropic chemical shift of the **1α** crystal phase that was taken as the reference. The linear regression shown in Figure S1 of the Supporting Information yielded R^2 values of 0.999 and 0.978 for ^{13}C and ^{1}H, respectively.

The computed ^{13}C isotropic chemical shifts were then employed to simulate the corresponding MAS NMR spectra of all the crystal forms, by means of a homemade code based on the resolution of spin effective Hamiltonians.[49]

The ^{1}H MAS NMR spectra were not simulated because the broadening effects due to the homonuclear dipole−dipole interactions, which are not averaged out in the experimental spectra reported in the literature,[6] are not included in the present version of our code.

RESULTS AND DISCUSSION

1α and 1·H$_2$O Crystal Forms. *Fully Optimized Structures.* The 1α phase belongs to a monoclinic system ($P2_1/n$), it contains four molecules of [(*p*-cymene)Ru(κN-INA)Cl$_2$] per unit cell (164 atoms), and it is characterized by intermolecular interactions represented by the −COOH···Cl− hydrogen bond along the 2_1 axis, which involve two consecutive molecules arranged in two alternate zigzag chains (a side view is displayed in Figure 1).

The inclusion of water (four molecules per unit cell) has a strong structural role in the packing of **1·H$_2$O**, since it organizes the half-sandwich units in water-assisted centrosymmetric supramolecular dimers. The water molecules bridge pairs of carboxylic groups by the OH···O and OH···Cl interactions: the metal−arene wheels interact together, forming the "inverted piano-stool" supramolecular motif,[2] which is clearly shown in Figure S2 of the Supporting Information.

Cell, Intra- and Intermolecular Parameters. An extensive analysis of the full optimized geometry of the **1α** and **1·H$_2$O** crystal forms, performed by using the hybrid B3LYP functional,[38,39] its combination with the "classical" Grimme dispersion correction (B3LYP-D2),[24] and the alternative reparametrization of the Grimme D2 term devised for crystals (B3LYP-D*)[40] has been carried out; the results are reported in detail in Tables S1 and S2 and in Figure S3 of the Supporting Information. Since the B3LYP-D* functional provides the best performance in reproducing the experimental structure, for brevity, only the results obtained by the B3LYP-D* full optimization are given in Tables 1 and 2.

dx.doi.org/10.1021/ic5006743 | Inorg. Chem. 2014, 53, 7926−7935

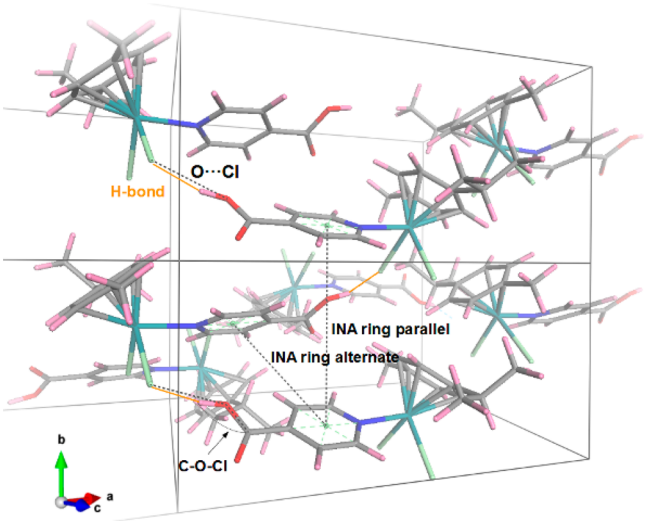

Figure 1. Perspective view of the **1α** polymorph (B3LYP-D*), with the continuous black line representing the unit cell. The Cl···O distance and the C−O—Cl angle are displayed, and hydrogen bonds are highlighted by orange lines. The distance between two INA rings belonging to two parallel equal layers (along *b*) or to two alternate neighboring layers (along *c*) is denoted by "INA ring parallel", and "INA ring alternate", respectively.

Table 1. Cell Parameters and Important Angles and Distances of the 1α Polymorph Obtained from Full Geometry Optimizations[a]

	B3LYP-D*	exptl[b]
a (Å)	14.890 (−0.867)	15.020
b (Å)	7.200 (−1.013)	7.274
c (Å)	15.123 (−2.433)	15.500
β (deg)	95.726 (0.287)	95.452
V (Å^3)	1613.20 (−4.304)	1685.75
Cl···O (Å)	3.037 (0.004)	3.033
C−O−Cl (deg)	112.435 (1.538)	113.973
N−Ru−*p*-cymene (deg)	127.166 (0.188)	127.354
Ru−*p*-cymene (Å)	1.685 (0.016)	1.669
Cl−Ru−Cl (deg)	86.770 (0.629)	86.141
INA ring parallel (Å)	7.200 (0.074)	7.274
INA ring alternate (Å)	5.030 (0.075)	5.105

[a]Percent relative deviations are reported in parentheses for the cell parameters, and absolute deviations are reported in parentheses for the distances and angles. [b]From ref 2.

Overall, the cell parameters of the **1α** polymorph are very well reproduced, the absolute errors being of less than 2.4%. The results obtained for the **1·H$_2$O** form can be considered satisfactory, although the angle *β* presents considerable deviations, and the volume of the unit cell for the optimized structure is smaller than the experimental value. This is probably due to a wrong inclusion of the long-range tail of the electrostatic part of H-bond interactions as dispersive interactions.

Some relevant **1α** polymorph distances and angles are also given in Table 1, together with their absolute deviation from the experimental data. The −Cl···(H)O distance (from now on referred as Cl···O) and the C−O(−H)···Cl− angle (from now on referred as C−O−Cl) are used to characterize the hydrogen bond length and angle of the **1α** phase, respectively (Figure 1). In the same way, for **1·H$_2$O** (Table 2), the H$_2$O oxygen−

Table 2. Cell Parameters and Important Angles and Distances of the 1·H$_2$O Form Obtained from Full Geometry Optimizations[a]

	B3LYP-D*	exptl[b]
a (Å)	15.146 (−3.684)	15.725
b (Å)	15.753 (−0.544)	15.839
c (Å)	7.257 (−2.204)	7.420
β (deg)	87.830 (4.280)	84.225
V (Å^3)	1730.14 (−5.908)	1838.78
H$_2$O···(H)O (Å)[c]	2.542 (0.014)	2.556
HO(H)···O (Å)[d]	2.781 (0.027)	2.808
HO(H)···Cl (Å)[e]	3.103 (0.007)	3.110
N−Ru−*p*-cymene (deg)	129.061 (0.115)	128.946
Ru−*p*-cymene (Å)	1.685 (0.017)	1.668
Cl−Ru−Cl (deg)	86.873 (0.856)	86.017
INA ring parallel (Å)	7.257 (0.163)	7.420
INA ring alternate (Å)	3.880 (0.089)	3.969

[a]Percent relative deviations are reported in parentheses for the cell parameters, and absolute deviations are reported in parentheses for the distances and angles. [b]From ref 2. [c]H bond between water oxygen and −COOH oxygen (hydrogen). [d]H bond between water oxygen (hydrogen) and −COOH oxygen. [e]H bond between water oxygen (hydrogen) and chlorine.

chlorine distance (HO(H)···Cl), and two oxygen−oxygen distances (H$_2$O···(H)O; HO(H)···O) are considered (both the water molecule and the carboxyl moieties give rise to H bonds by using both their H and O atoms; see Figure S2 in the Supporting Information). Moreover, two intermolecular parameters, which represent the INA arene-stacking distances depicted in Figure 1, are reported in Tables 1 and 2. Both the "parallel" and the "alternate" configurations have been measured (INA ring parallel and INA ring alternate). If it is considered that long distances (3−4 to 7−9 Å) are involved, these parameters may give an idea of the structural impact of long-range dispersive effects.

It can be observed from the data given in Table 1 that the Cl···O distance of **1α** is well described, whereas major errors affect the related C−O−Cl angle (about 1.5°), thus resulting in uncertainty about the position of the −OH groups involved in the H bond.

Unexpectedly, the parameters involving the Ru(II) atom are predicted with acceptable errors for both crystal forms at all levels of approximation used in the minimization of the crystal forms (see Tables S1 and S2 of the Supporting Information).

^{13}C and ^{1}H NMR Calculations. The ^{13}C MAS NMR spectra of the **1α** and **1·H$_2$O** forms simulated by using the ^{13}C isotropic chemical shifts computed on the B3LYP-D* optimized geometries are shown in Figure 2, together with their respective experimental spectra.[2] The corresponding labeling scheme adopted is shown in Figure 3. A deeper comparison of the results obtained by means of the structures minimized with different functionals is reported in the Supporting Information.

Overall, a satisfactory agreement is found, notwithstanding the perceivable peak shifts at 150−160 and ∼138 ppm in the ^{13}C MAS NMR theoretical spectrum of the **1α** structure and the marked peak splitting at ∼120, ∼100, and ∼80 ppm in the ^{13}C MAS NMR spectrum of the **1·H$_2$O** form, not detectable by the experiment (Figure 2). This can be ascribed to the omission of thermal effects (calculations refer to 0 K) which are intrinsically present in the experiments.

dx.doi.org/10.1021/ic5006743 | Inorg. Chem. 2014, 53, 7926−7935

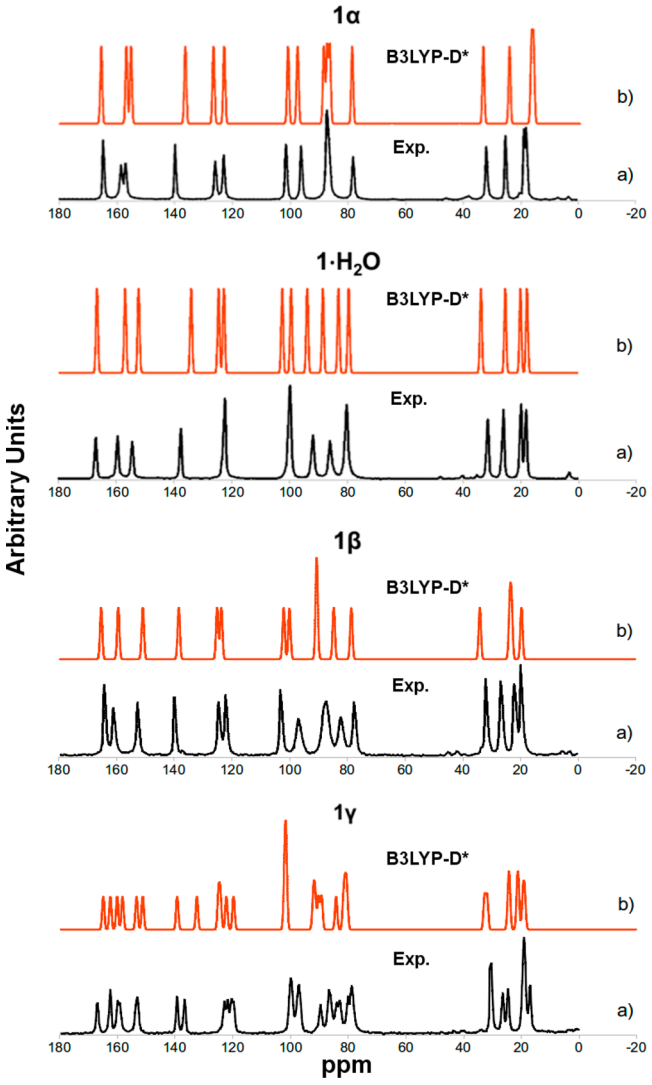

Figure 2. Simulated and experimental ^{13}C solid-state NMR spectra of the **1*α***, **1·H$_2$O**, **1*β***, and **1*γ*** forms.

Further insights can be obtained by the analysis of the mean absolute deviations (MAD) between the computed and experimental ^{13}C chemical shifts (δ_{iso}) data values of the **1*α*** and **1·H$_2$O** crystal forms.

MADs are computed as $(\sum_n|(\delta_{iso,n}(computed) - \delta_{iso,n}(experimental)|)/n$ and are given in Table 3 for the B3LYP-D* optimized geometries. Overall, a good agreement is detected, the MAD being 1.3 ppm for **1*α*** and 1.9 ppm for **1·H$_2$O**. A slightly larger deviation is expected for the **1·H$_2$O** chemical shifts, since the δ_{iso} scale was set by using the **1*α*** structure. However, it is worth stressing that a major difference is noted between the computed and experimental ^{13}C δ_{iso} assignments of the C1 and C5 atoms of **1·H$_2$O**. This implies a rotation of the whole INA moiety (C2 and C4 δ_{iso} values are experimentally equivalent). In fact, as is clearly shown in Figure 4a,b, the mutual positions of the −COOH and *p*-cymene isopropyl groups in the **1·H$_2$O** phase (C4−C3−C6−O1(H) −169.20°) are almost opposite with respect to those of the **1*α*** polymorph (C4−C3−C6−O1(H) dihedral angle being 17.92°). Figure 4 shows the fully optimized structures; however, this situation is present also in the experimental nonrefined structures, but it has not been highlighted in

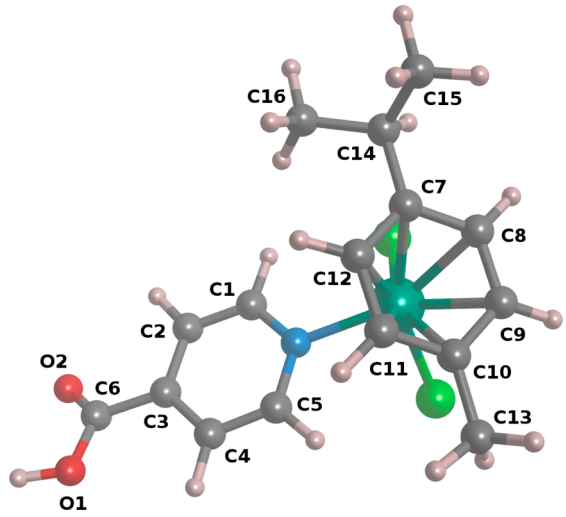

Figure 3. Molecular structure and labeling scheme of [(*p*-cymene)-Ru(*κ*N-INA)Cl$_2$]. The original NMR labeling from ref 2 for the carbon and oxygen atoms of the **1*α*** polymorph is shown. The **1·H$_2$O** and **1*β*** polymorphs and the two molecules of the **1*γ*** polymorphs are labeled accordingly, independent of the mutual position of the −COOH and isopropyl groups (Figure 4).

previous works.[2,6] The recalculated MADs are reported in parentheses in Table 3 and result in a value of 1.6 ppm.

For the ^1H NMR isotropic chemical shifts given in Table 4, the MADs computed for H1 and H5 δ_{iso} data are almost invariant. However, a marked deviation of about 7 ppm of the signal of H (OH), which corresponds to the hydrogen atom belonging to the carboxyl group in **1·H$_2$O**, should be highlighted. This discrepancy is probably due to a possible proton exchange with the water molecules that can occur during experiments and that is not taken into proper account by means of static calculations. A deeper investigation of the proton exchange and of its effects on the ^1H chemical shifts should be based on molecular dynamics simulations that intrinsically include thermal effects.[50−52]

An extensive comparison of the results obtained by means of different levels of theory is reported in Tables S3 and S4 of Supporting Information.

1*β* Polymorph. *Fully Optimized Structure.* The **1*β*** polymorph ($P2_1/c$, 164 atoms per cell) is characterized by two layers containing an intermolecular −COOH···Cl interaction, which lies in the *ab* plane (Figure S5, Supporting Information). Though its structure is similar to that of **1·H$_2$O**, the **1*β*** phase presents the same kind of H bond (−COOH··· Cl) that belongs to the **1*α*** polymorph.

Cell Intra- and Intermolecular Parameters. The cell parameters obtained by B3LYP-D* full geometry optimizations and their percent relative deviations from experimental data are given in Table 5. The final cell is more compact than the experimental one, since the overestimation of the *b* and *β* parameters compensates for the symmetry change due to *a* and *c*. The H-bond pattern along *a* prevails over the *b* direction. In the same way, the superposition of aromatic groups provides a strong directionality to long-range correlation effects, consequently giving an underestimation of *c*.

The results for the inter- and intramolecular parameters, also given in Table 5, underline a slight change of the N−Ru−*p*-cymene and C−O−Cl angles (0.7 and 0.8°, respectively), whereas the Cl−Ru−Cl angle is wider than the experimental

dx.doi.org/10.1021/ic5006743 | Inorg. Chem. 2014, 53, 7926−7935

Table 3. Computed (Fully Optimized Structures) and Experimental ^{13}C Chemical Shifts of the Four Crystalline Forms of [(*p*-cymene)Ru(*κ*N-INA)Cl_2]

	δ_{iso} (ppm)							
	1*α* form		**1·H_2O** form		**1*β*** form		**1*γ*** form	
	B3LYP-D*	exptl[a]	B3LYP-D*	exptl[a]	B3LYP-D*	exptl[a]	B3LYP-D*	exptl[b]
C1	155.4	156.9	152.4	**159.6**[d]	151.1	152.9	151.4/153.5	**160.3/159.5**[d]
C2	126.8	125.8	124.5	122.6	123.9	122.2	122.4/125.1	**120.8/120.0**[d]
C3	136.6	139.7	134.2	137.7	138.7	140.1	139.4/132.5	139.7/137.1
C4	123.1	122.8	122.7	122.6	125.2	124.8	124.4/119.8	**123.3/122.2**[d]
C5	157.0	158.4	157.0	**154.5**[d]	159.6	161.4	158.5/160.3	**153.8/153.3**[d]
C6	165.8	164.6	166.7	167.2	165.7	164.5	165.2/162.7	167.3/162.9
C7	101.1	101.2	99.4	100.1	102.2	103.1	101.6/101.9	100.5/99.9
C8	88.7	86.9	93.9	92.1	90.7	**77.6**[d]	92.2/91.6	79.2
C9	87.7	86.9	88.5	86.1	90.7	**82.4**[d]	89.3/90.3	89.9/87.0
C10	97.8	96.0	102.5	100.1	100.1	97.1	102.2/101.5	97.4
C11	86.7	86.3	83.1	80.5	84.8	**87.8**[d]	81.1/84.3	86.5/84.3
C12	79.0	77.9	79.6	80.5	78.7	**87.3**[d]	81.7/80.5	83.2/80.5
C13	16.8	17.7	19.9	20.2	19.6	19.4	20.9/19.3	19.2/17.3
C14	33.5	31.7	33.6	31.7	34.0	31.8	31.8/32.7	30.8
C15	24.4	25.0	25.1	26.3	23.6	21.9	23.9/24.4	26.8/24.9
C16	16.0	18.6	17.6	18.4	23.0	26.5	18.8/21.2	19.2
MAD[c]	**1.3**		**1.9(1.6)**[d]		**3.3(1.8)**[d]		**3.1(2.3)**[d]	

[a]From ref 2. [b]From ref 6. [c]Mean absolute deviations (reported in boldface). For **1*γ***, MADs are calculated on the mean of δ_{iso} data values of molecules (**1**) and (**2**). [d]The exchange of C1/C5 δ_{iso} values for **1·H_2O**, C8/C12 and C9/C11 δ_{iso} values for **1*β***, and C1/C5 and C2/C4 δ_{iso} values for **1*γ*** (reported in boldface) yields the MADs reported in parentheses.

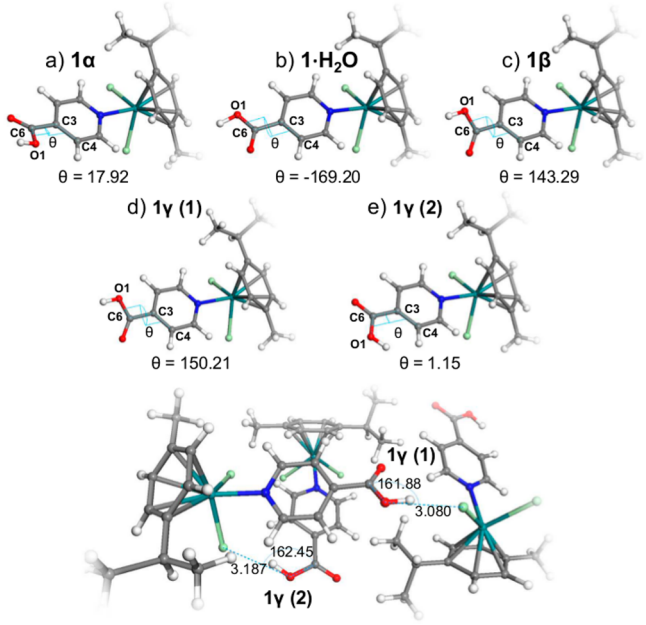

Figure 4. (top) Comparison between the −COOH group structural positions of the different polymorphs (fully optimized geometries): (a) **1*α***; (b) **1·H_2O**; (c) **1*β***; (d, e) the two molecules (**1**) and (**2**), respectively, of **1*γ***. (bottom) The two H bonds in the **1*γ*** form (fully optimized geometry), highlighted with dotted lines.

value of about 7°. The Cl−Ru−Cl moiety lies perpendicular to the *c* direction, along which the interplay of the H-bond network and vdW forces result in an overestimation of the cell packing.

Although the errors in all the distance parameters are small and fall within ∼0.3 Å, it is worth noting the large absolute percent relative deviations of the Cl···O distance (involving the hydrogen bond) displayed in Figure S6 (Supporting Information), which is comparable to the absolute percent relative deviations of the Cl−Ru−Cl angle.

^{13}C and ^{1}H NMR Calculations. Figure 2 allows the comparison of the ^{13}C MAS NMR experimental spectrum of the **1*β*** polymorph with the computed spectrum. Moreover, the computed ^{13}C and ^{1}H chemical shifts (δ_{iso}) are given in Tables 3 and 4, together with the experimental values.[2]

The impact of geometry optimization of the XRPD **1*β*** structure on the agreement between theoretical and experimental spectra is notable. Full details are available in the Supporting Information. Briefly, the agreement between the δ_{iso} data values calculated for the nonrefined XRPD experimental structure and the experimental structure is poor. The optimization of H atoms ameliorates significantly the ^{13}C and ^{1}H δ_{iso} data values and the ^{13}C spectrum with respect to the nonrefined values, while only minor differences are observed when the hydrogen-optimized and fully optimized spectra are compared.

Importantly, the computed δ_{iso} data values of the aromatic −CH− groups (Tables 3 and 4) seem to be in better agreement with the experiment if the δ_{iso} assignments of the C9 and C8 carbon atoms (which belong to the INA *p*-cymene ring) are interchanged with those of C11 and C12, respectively. In fact, the MAD values for the $^{13}C/^{1}H$ NMR signals after the 8/12 and 9/11 atom exchange are MAD(^{13}C) = 1.8 ppm MAD(^{1}H) = 0.5 ppm. These figures underline a significant improvement with respect to the assignment by Chierotti et al.,[6] which yields MAD(^{13}C) = 3.3 ppm and MAD(^{1}H) = 0.6 ppm (see Tables 3 and 4).

To support this hypothesis, it is worth recalling that Chierotti et al.[6] detected uncertainty in the aromatic hydrogens and labeled the assignments of ^{1}H δ_{iso} as H9/H11, H11/H9, H8/H12, and H12/H8. However, in the present work the original atom labeling from ref 2 has been retained (Figure 3).

1*γ* Polymorph. *Fully Optimized Structure.* The phase **1*γ*** belongs to the $P2_1/a$ space group, a nonstandard setting of $P2_1/$

dx.doi.org/10.1021/ic5006743 | Inorg. Chem. 2014, 53, 7926−7935

Table 4. Computed (Fully Optimized Structures) and Experimental ^{1}H Chemical Shifts of the Four Crystalline Forms of [(*p*-cymene)Ru(κN-INA)Cl$_2$]

	δ_{iso} (ppm)							
	1α form		**1·H$_2$O** form		**1β** form		**1γ** form	
	B3LYP-D*	exptl[a]	B3LYP-D*	exptl[a]	B3LYP-D*	exptl[a]	B3LYP-D*	exptl[b]
H1	8.8	9.4	8.0	**8.6**[d]	7.7	8.5	8.2/8.3	**9.1**[d]
H2	8.8	8.7	7.2	**6.3**[d]	7.0	7.1	7.1/7.1	**7.1**[d]
H4	6.4	6.2	6.4	**6.7**[d]	7.2		7.1/7.4	**6.6/6.5**[d]
H5	7.8	8.6	8.3	**8.9**[d]	8.4	9.1	8.4/8.9	**8.8/8.9**[d]
H(OH)	10.2	9.9[b]	15.6	8.7	10.8	10.1	11.0/10.6	10.5
H8	4.8	4.6	5.7	5.8	5.4	**5.3**[d]	5.6/5.9	5.0
H9	4.2	4.6	5.4	5.9	5.5	**4.8**[d]	5.7/5.5	5.5
H11	4.9	5.0	4.5	5.1	4.6	**6.0**[d]	4.7/4.8	5.6/5.4
H12	4.7	4.8	5.2	5.1	5.5	**5.5**[d]	5.1/5.3	5.0/5.4
H13[e]	2.7	2.5	2.3	1.8	2.5	1.8	2.6/2.6	1.7/1.4
H14	3.2	3.2	3.3	3.1	3.3	3.2	4.2/3.4	3.2
H15[e]	1.5	1.2	2.0	1.4	2.3	1.2	2.3/2.3	1.8/1.6
H16[e]	0.6	0.5	1.7	1.3	1.3	1.6	1.6/1.2	1.4
MAD[c]	**0.3**		**0.9(0.9)**[d]		**0.6(0.5)**[d]		**0.5(0.5)**[d]	

[a]From ref 2. [b]From ref 6. [c]Mean absolute deviations (reported in boldface). For **1γ**, MADs are calculated on the mean of δ_{iso} data values of molecules (**1**) and (**2**). [d]The exchange of H1/H5 and H2/H4 δ_{iso} values for **1·H$_2$O**, H8/H12 and H9/H11 δ_{iso} values for **1β**, and H1/H5 and H2/H4 δ_{iso} values for **1γ** (reported in boldface) yields the MADs reported in parentheses. [e]Only one experimental δ_{iso} data value is given for the three H atoms of CH_3 groups (H13, H15, and H16); the mean value is reported for the computed data.

Table 5. Cell Parameters and Important Angles and Distances of the **1β** Polymorph Obtained from Full Geometry Optimizations[a]

	B3LYP-D*	exptl[b]
a (Å)	14.103 (−4.092)	14.705
b (Å)	15.444 (2.375)	15.086
c (Å)	7.410 (−4.054)	7.723
β (deg)	99.936 (1.928)	98.046
V (Å^3)	1589.91 (−6.28)	1696.54
Cl···O (Å)	3.130 (0.294)	3.424
C−O−Cl (deg)	124.006 (0.712)	123.294
N−Ru−*p*-cymene (deg)	129.081 (0.846)	128.235
Ru−*p*-cymene (Å)	1.687 (0.019)	1.668
Cl−Ru−Cl (deg)	87.943 (7.395)	80.548
INA ring parallel (Å)	7.410 (0.313)	7.723
INA ring alternate (Å)	3.792 (0.158)	3.950

[a]Percent relative deviations are reported in parentheses for the cell parameters, and absolute deviations are reported in parentheses for the distances and angles. [b]From ref 6.

c for which the polymorph contains two molecules of [(*p*-cymene)Ru(κN-INA)Cl$_2$] in the asymmetric unit (8 molecules/328 atoms per cell). Substantial differences in the spatial position of the −COOH group in the two molecular units are observed.

A description of the fully optimized structures is given in Figure 5, where a comparison with the nonrefined XRPD experimental structure, used as input, is also reported.

A comparison among the four crystal forms furnishes interesting information (Figure 4): the −COOH moiety of the **1α** polymorph is almost planar with respect to the INA ring, the C4−C3−C6−O1(H) dihedral angle being 17.92° (Figure 4a). As explained in the previous section, in the **1·H$_2$O** phase a substantial rotation of the −COOH group is observed (C4−C3−C6−O1(H) −169.20°; Figure 4b), whereas the C4−C3−C6−O1(H) dihedral angle of the **1β** polymorph is 143.29° (Figure 4c).

The first molecule in the fully optimized structure of the **1γ** polymorph, (also referred as (**1**) in the following) (Figure 4d), being characterized by the −COOH dihedral angle of 150.21° skewed with respect to the INA ring, is similar to the **1β** form (Figure 4c). The second molecule (also referred as (**2**) in the following) (Figure 4e) presents a dihedral angle of 1.15° (almost planar) which is comparable to that of **1α** (Figure 4a), although the acidic hydrogen points in a different direction with respect to the **1α** polymorph.

In both molecules of the **1γ** polymorph, the acidic hydrogen establishes an H···Cl bond with similar geometry, as highlighted in Figure 5: the O···Cl distances are 3.080 and 3.187 Å for molecules (**1**) and (**2**), respectively, and the O−H···Cl angles are 161.88 and 162.45° for molecules (**1**) and (**2**), respectively. This is reflected also by the electron charge density of the H and Cl atoms involved in the COOH···Cl interaction. A qualitative pictorial analysis for the three fully optimized (B3LYP-D*) anhydrous polymorphs is given in Figure 6. The Bader atomic volumes of the charge density around H and Cl atoms, partitioned according to Bader's quantum theory of atom in molecules (QTAIM),[53] are depicted with an isosurface density value of 0.02 a_0^{-3}. The figure shows that the partial charge on H atoms tends to delocalize in the direction of acceptors (Cl atoms) and the charge densities for the H···Cl interaction are similarly shaped for the four molecules, supporting the hypothesis that the two H bonds present in the 1γ phase have similar strengths.

Indeed, both the nonrefined XRPD experimental structure (Figure 5) and the results of the refined XRPD/NMR/DFT structural characterization[6] furnish a detectable difference in the geometry of the O−H···Cl moiety. In fact, the O···Cl distances are 3.103/3.170 Å (Figure 5) and 3.085/3.183 Å, and the O−H···Cl angles are 162.65/151.48° (Figure 5) and 156.2/166.2° for the molecules (**1**) and (**2**) of the nonrefined XRPD experimental and refined XRPD/NMR/DFT structures,[6] respectively. This evidence led Chierotti et al.[6] to hypothesize the presence of one strong H···Cl bond and a weaker H···Cl contact in the **1γ** polymorph. Nonetheless, the structure and

dx.doi.org/10.1021/ic5006743 | Inorg. Chem. 2014, 53, 7926−7935

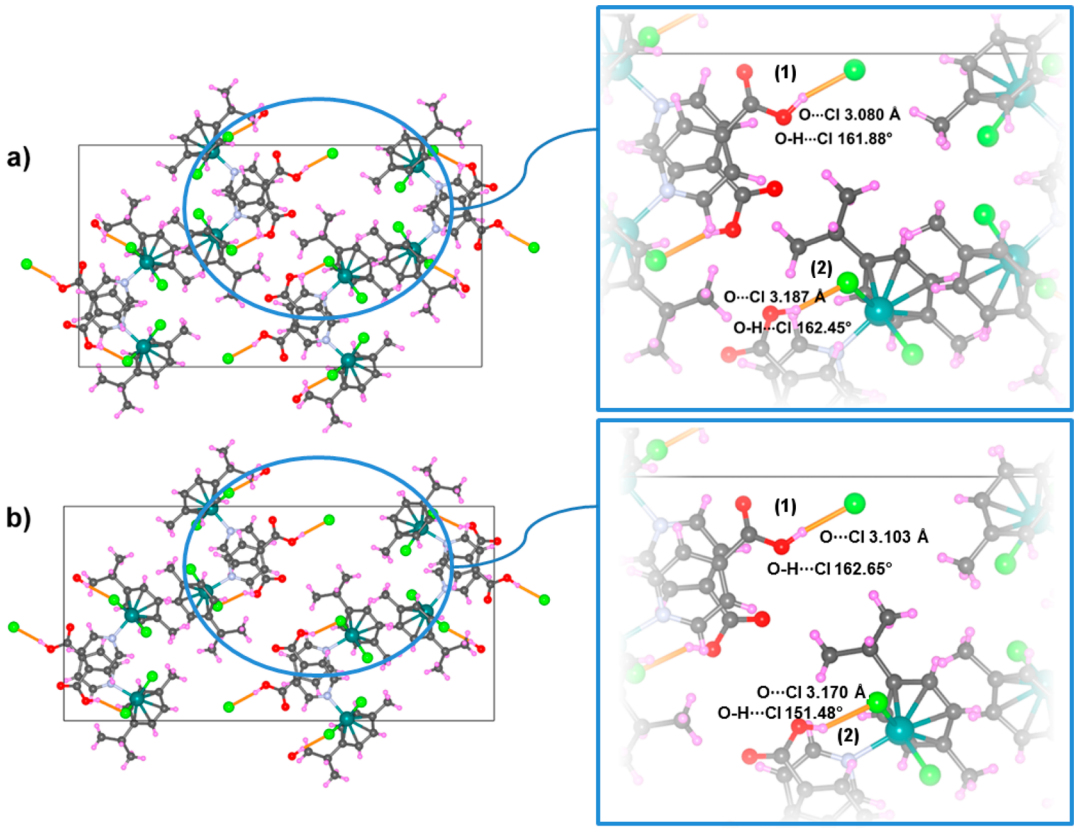

Figure 5. *ab* plane view of (a) the fully optimized structure (B3LYP-D*) of the **1γ** form and (b) the nonrefined XRPD experimental structure used as input for calculations.

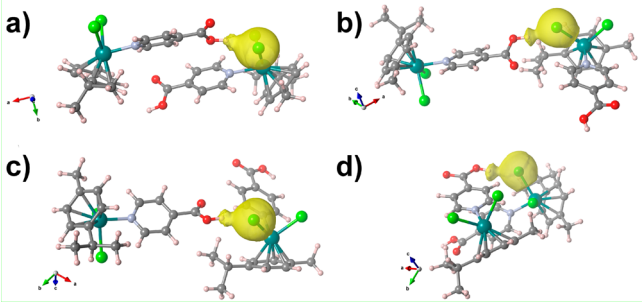

Figure 6. Atomic volume partitioning of the Bader charge around the atoms involved in the COOH···Cl interaction for the (a) **1α**, (b) **1β**, (c) **1γ(1)**, and (d) **1γ(2)** crystal forms. The yellow surface around the H and Cl atoms is represented with an isosurface density value of 0.02 a_0^{-3}. The original charge density has been partitioned through the software "Bader".[54−56]

labeling of molecule **(2)** in the asymmetric unit was not reported in ref 6.

Cell Inter- and Intramolecular Parameters. The full geometry optimization leads to minor changes in cell parameters. The direction *a*, along which both H bonds and dispersive interactions are present, constitutes an exception, being underestimated by 2.4 Å (Table 6). As for **1β**, the INA rings of alternate layers are aligned along *c*.

Marked absolute percent relative deviations on intermolecular parameters are related to the C−O−Cl angle (C−O−Cl 3.6° for **(1)** and 9.9° for **(2)**), which involves the hydrogen bonds (Figure S8, Supporting Information). Moreover, a considerable discrepancy with the experimental structure is

Table 6. Cell Parameters and Important Angles and Distances of the 1γ Polymorph Obtained from Full Geometry Optimizations[a]

	B3LYP-D*	exptl[b]
a (Å)	28.557 (−7.630)	30.916
b (Å)	15.613 (1.773)	15.341
c (Å)	7.309 (−0.791)	7.368
β (deg)	95.980 (0.740)	95.275
V (Å^3)	3241.32 (−6.85)	3479.64
Cl···O (Å)		
(1)	3.080 (0.023)	3.103
(2)	3.187 (0.017)	3.170
C−O−Cl (deg)		
(1)	124.802 (3.604)	128.406
(2)	130.037 (9.957)	139.994
N−Ru−*p*-cymene (deg)		
(1)	128.440 (2.388)	126.052
(2)	128.286 (4.337)	132.623
Ru−*p*-cymene (Å)		
(1)	1.685 (0.017)	1.668
(2)	1.690 (0.022)	1.668
Cl−Ru−Cl (deg)		
(1)	88.756 (3.213)	85.543
(2)	87.368 (3.708)	83.660
INA ring parallel (Å)	7.309 (0.059)	7.368
INA ring alternate (Å)	3.798 (0.037)	3.835

[a]Percent relative deviations are reported in parentheses for the cell parameters, and absolute deviations are reported in parentheses for the distances and angles. [b]From ref 6.

dx.doi.org/10.1021/ic5006743 | Inorg. Chem. 2014, 53, 7926−7935

observed for the optimized Cl−Ru−Cl intramolecular angle (overestimated by ∼3°). Such rearrangement competes with ring-stacking dispersive interactions to the mild shortening of the *c* direction. Substantial differences are observed also for the N−Ru−*p*-cymene angle (+2.4°/−4.3° for molecules (**1**) and (**2**), respectively).

^{13}C and ^{1}H NMR Calculations. The simulated ^{13}C MAS NMR spectra of the **1*γ*** polymorph computed on the refined structure is shown in Figure 2, and the calculated ^{13}C and ^{1}H chemical shifts (δ_{iso}) are given in Tables 3 and 4. An extensive comparison of the results obtained by means of the structures minimized with different functionals is reported in the Supporting Information.

The presence of two molecules of [(*p*-cymene)Ru(*κ*N-INA)Cl_2] in the asymmetric unit, almost indistinguishable in the experimental spectra, yields two different sets of δ_{iso} data values for the calculated parameters and a manifold ^{13}C spectrum, where many peaks are overlapped.

Therefore, the agreement between the experimental and simulated spectra can be considered only qualitative.

Importantly, more accuracy in the peak position of the carbon atoms belonging to the ring carrying the −COOH group of the two molecules (Table 3) is achieved when the δ_{iso} data value assignment of the aromatic C1 is exchanged with its equivalent atom C5, and C2 with C4. This is highlighted by the values of the MADs calculated by considering the mean δ_{iso} data values of molecules (**1**) and (**2**), both with the original assignment and after the exchange.

A comparison between the computed and experimental ^{1}H δ_{iso} data values (Table 4) is difficult, since the broad experimental signals impede the discrimination and assignments of most of the ^{1}H resonances for the symmetry-nonequivalent molecules. However, in general, the same considerations made for the ^{13}C δ_{iso} data values hold also in this case.

Interestingly, a broad signal centered at 10.5 ppm was detected for the −COOH hydrogen (H6) in the experimental MAS spectrum recorded by Chierotti et al.[6] This signal presents a reduced intensity with respect to the corresponding signal in the **1*β*** polymorph. Thus, the authors hypothesized the presence of a second weak hydrogen bond, whose signal is supposed to fall in the region characteristic of the pyridine protons. This hypothesis was supported by the results of a NMR-GIAO DFT calculation, which yielded ^{1}H δ_{iso} data values of 12.2 and 9.6 ppm for the strong and weak interactions, respectively. However, no signal is present at 12.2 ppm in the experimental spectrum. Moreover, the more accurate NMR-GIPAW DFT calculations carried out in this work on the nonrefined experimental geometry (Figure S9, Supporting Information) yields a very different result: ^{1}H δ_{iso} values of 9.5 and 9.4 ppm for the acidic hydrogen of the two molecules. These discrepancies suggest that, as pointed out previously, the experimental geometry might require further refinement. In fact, it is worth recalling that the experimental structure was obtained by an iterative XRPD-DFT calculation procedure and no correction for dispersion effects was included in the periodic lattice DFT calculations.[6]

Moreover, NMR-GIPAW DFT calculations on the refined XRPD/NMR/DFT structure reported by Chierotti et al.[6] provide ^{1}H δ_{iso} data values of 11.0 and 10.9 ppm for the strong and weak H bonds and are in disagreement with the DFT-GIAO results.

These results reflect the differences in the accuracy of the two theoretical approaches and suggest that the peaks of both hydrogen atoms engaged in the formation of H bonds lie in the same spectral regions. That is, the peak of the second hydrogen does not fall overlapped under the signals of aromatic hydrogen atoms in ortho positions with respect to the pyridine nitrogen atoms, as hypothesized by Chierotti et al.[6]

The NMR-GIPAW DFT calculations carried out in this work on the structures optimized by including the dispersion corrections furnish results more comparable with the experimental data, as testified to by the impressive agreement with the ^{1}H−^{13}C FSLG-HETCOR spectrum shown in Figure 7.

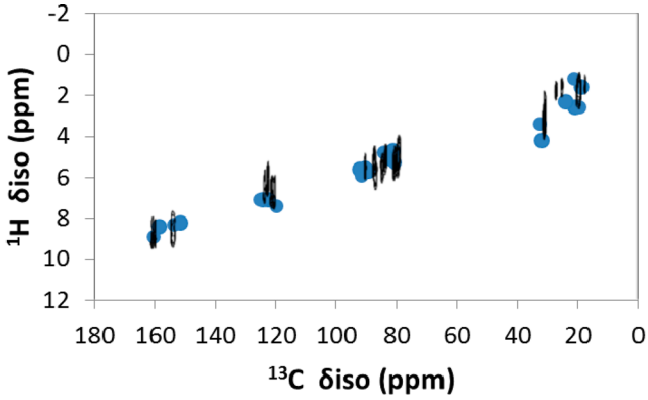

Figure 7. Superposition of the ^{1}H−^{13}C FSLG-HETCOR spectrum obtained for the **1*γ*** crystal form (in black; ref 6) and the correlated ^{1}H−^{13}C NMR parameters (blue dots) obtained by means of the NMR-GIPAW DFT calculations on the B3LYP-D* fully optimized structure.

In particular, the ^{1}H δ_{iso} data values computed for the −COOH hydrogen (H6) after hydrogen relaxation (Table S6, Supporting Information) are 10.4/10.6 ppm for molecules (**1**)/(**2**), respectively. Slightly different values (11.0/10.6 ppm for molecules (**1**)/(**2**), respectively) are obtained also in the case of the fully relaxed structure (Table 4 and Table S6), once again endorsing the hypothesis of two distinct COOH···Cl bonds of comparable strength.

CONCLUSIONS

The ^{13}C/^{1}H NMR parameters and ^{13}C MAS NMR spectra of the **1*α***, **1·H_2O**, **1*β***, and **1*γ*** forms of [(*p*-cymene)Ru(*κ*N-INA)Cl_2] have been calculated by means of the PBE-GIPAW method.

The results showed that, in order to obtain good agreement with the spectroscopic data, full geometry optimizations of the experimental structures or, at least, computational refinement of the hydrogen atoms is mandatory. Moreover, addition of a dispersion correction term (the "classical" Grimme dispersion correction −D2 or its alternative reparametrization devised for crystals −D*) to the pure B3LYP functional used, under periodic boundary conditions, for the geometry optimization protocol is extremely important to ameliorate the structure and spectra prediction.

The experimental and computed ^{13}C and ^{1}H δ_{iso} data value differences, expressed as mean absolute deviations, lie in the ranges 1.3−2.9 and 0.3−1.0 ppm, respectively. Furthermore, some revisions in the experimental assignment of the ^{13}C/^{1}H NMR δ_{iso} parameters of the **1·H_2O**, **1*β***, and **1*γ*** forms have been suggested. The mismatch in the assignment seems to be mainly

dx.doi.org/10.1021/ic5006743 | Inorg. Chem. 2014, 53, 7926−7935

due to the rotation of the −COOH moiety, which occurs at the **1α**−**1**·H_2O transition and was not considered in the experiments.

Finally, the results obtained suggest the presence of two COOH···Cl hydrogen bonds of comparable strength established by the two molecules in the asymmetric unit of the **1γ** polymorph, in partial disagreement with previous findings.

■ ASSOCIATED CONTENT

Supporting Information

Text, tables, and figures giving the linear regression for $^{13}C/^{1}H$ NMR δ_{iso} of **1α** as well as the descriptions and figures of the four crystalline structures, all of the computed $^{13}C/^{1}H$ NMR δ_{iso} values with the related ^{13}C spectra, and the calculated $^{13}C/^{1}H$ NMR correlation spectra. This material is available free of charge via the Internet at http://pubs.acs.org.

■ AUTHOR INFORMATION

Corresponding Authors

*E-mail for A.P.: alfonso.pedone@unimore.it.

*E-mail for M.C.M.: mariacristina.menziani@unimore.it.

Author Contributions

The manuscript was written through contributions of all authors. All authors have given approval to the final version of the manuscript.

Notes

The authors declare no competing financial interest.

■ ACKNOWLEDGMENTS

The authors acknowledge Prof. Alessia Bacchi for the nonrefined structures of **1β** and **1γ** and Dr. Ilaria Ciofini for useful discussions. D.P. thanks Regione Emilia-Romagna for financial support through the SPINNER 2013 program entitled "Ottimizzazione delle forme molecolari e crystalline di farmaci, fitofarmaci, pesticidi in relazione ad attività, biodisponibilità aspetti brevettuali, e alla produzione di polimorfi, solvati e cocrystalli con metodi a basso impatto ambientale".

■ REFERENCES

(1) Soldatov, D. V. *J. Chem. Crystallogr.* **2006**, *36*, 747−768.

(2) Bacchi, A.; Cantoni, G.; Chierotti, M. R.; Girlando, A.; Gobetto, R.; Lapadula, G.; Pelagatti, P.; Sironi, A.; Zecchini, M. *CrystEngComm* **2011**, *13*, 4365−4375.

(3) Bacchi, A.; Bosetti, E.; Carcelli, M.; Pelagatti, P.; Rogolino, D. *Eur. J. Inorg. Chem.* **2004**, *10*, 1985−1991.

(4) Bacchi, A.; Bosetti, E.; Carcelli, M.; Pelagatti, P.; Rogolino, D. *CrystEngComm* **2004**, *6*, 177−183.

(5) Bacchi, A.; Bosetti, E.; Carcelli, M.; Pelagatti, P.; Rogolino, D.; Pelizzi, G. *Inorg. Chem.* **2005**, *44*, 431−442.

(6) Chierotti, M. R.; Gobetto, R.; Nervi, C.; Bacchi, A.; Pelagatti, P.; Colombo, V.; Sironi, A. *Inorg. Chem.* **2014**, *53*, 139−146.

(7) Santos, S. M.; Rocha, J.; Mafra, L. *Cryst. Growth Des.* **2013**, *13*, 2390−2395.

(8) Többens, D. M.; Glinneman, J.; Chierotti, M. R.; van de Streek, J.; Sheptyakov, D. *CrystEngComm* **2012**, *14*, 3046−3055.

(9) Bonhomme, C.; Gervais, C.; Babonneau, F.; Coelho, C.; Pourpoint, F.; Azaïs, T.; Ashbrook, S. E.; Griffin, J. M.; Yates, J. R.; Mauri, F.; Pickard, C. J. *Chem. Rev.* **2012**, *112*, 5733−5779.

(10) Ashbrook, S. E.; Berry, A. J.; Frost, D. J.; Gregorovic, A.; Pickard, C. J.; Readman, J. E.; Wimperis, S. *J. Am. Chem. Soc.* **2007**, *129*, 13213−13224.

(11) Hinklin, T.; Toury, B.; Gervais, C.; Babonneau, F.; Gislason, J.; Morton, R.; Laine, R. *Chem. Mater.* **2004**, *16*, 21−30.

(12) Pedone, A.; Gambuzzi, E.; Menziani, M. C. *J. Phys. Chem. C* **2012**, *116*, 14599−14609.

(13) Pedone, A.; Charpentier, T.; Menziani, M. C. *J. Mater. Chem.* **2012**, *22*, 12599−12608.

(14) Charpentier, T.; Menziani, M. C.; Pedone, A. *RSC Adv.* **2013**, *3*, 10550−10578.

(15) Harris, R. K.; Ghi, P. Y.; Puschmann, H.; Apperley, D. C.; Griesser, U. J.; Hammond, R. B.; Ma, C.; Roberts, K. J.; Pearce, G. J.; Yates, J. R.; Pickard, C. J. *Org. Process Res. Dev.* **2005**, *9*, 902−910.

(16) Harris, R. K.; Hodgkinson, P.; Larsson, T.; Muruganantham, A.; Ymén, I.; Yufit, D. S.; Zorin, V. *Cryst. Growth Des.* **2008**, *8*, 80−90.

(17) Pickard, C. J.; Mauri, F. *Phys. Rev. B* **2001**, *63*, 245101.

(18) Yates, J. R.; Pickard, C. J.; Mauri, F. *Phys. Rev. B* **2007**, *76*, 024401.

(19) Brouwer, D. H.; Enright, G. D. *J. Am. Chem. Soc.* **2008**, *130*, 3095−3105.

(20) Brouwer, D. H. *J. Am. Chem. Soc.* **2008**, *130*, 6306−6307.

(21) Day, G. M.; Motherwell, W. D. S.; Ammon, H. L.; Boerrigter, S. X. M.; Della Valle, R. G.; Venuti, E.; Dzyabchenko, A.; Dunitz, J. D.; Schweizer, B.; van Eijck, B. P.; Erk, P.; Facelli, J. C.; Bazterra, V. E.; Ferraro, M. B.; Hofmann, D. W. M.; Leusen, F. J. J.; Liang, C.; Pantelides, C. C.; Karamertzanis, P. G.; Price, S. L.; Lewis, T. C.; Nowell, H.; Torrisi, A.; Scheraga, H. A.; Arnautova, Y. A.; Schmidt, M. U.; Verwer, P. *Acta Crystallogr., Sect. B* **2005**, *61*, 511−527.

(22) Day, G. M.; Cooper, T. G.; Cruz-Cabeza, A. J.; Hejczyk, K. E.; Ammon, H. L.; Boerrigter, S. X. M.; Tan, J. S.; Della Valle, R. G.; Venuti, E.; Jose, J.; Gadre, S. R.; Desiraju, G. R.; Thakur, T. S.; van Eijck, B. P.; Facelli, J. C.; Bazterra, V. E.; Ferraro, M. B.; Hofmann, D. W. M.; Neumann, M. A.; Leusen, F. J. J.; Kendrick, J.; Price, S. L.; Misquitta, A. J.; Karamertzanis, P. G.; Welch, G. W. A.; Scheraga, H. A.; Arnautova, Y. A.; Schmidt, M. U.; van de Streek, J.; Wolf, A. K.; Schweizer, B. *Acta Crystallogr., Sect. B* **2009**, *65*, 107−125.

(23) Bardwell, D. A.; Adjiman, C. S.; Arnautova, Y. A.; Bartashevich, E.; Boerrigter, S. X. M.; Braun, D. E.; Cruz-Cabeza, A. J.; Day, G. M.; Della Valle, R. G.; Desiraju, G. R.; van Eijck, B. P.; Facelli, J. C.; Ferraro, M. B.; Grillo, D.; Habgood, M.; Hofmann, D. W. M.; Hofmann, F.; Jose, K. V. J.; Karamertzanis, P. G.; Kazantsev, A. V.; Kendrick, J.; Kuleshova, L. N.; Leusen, F. J. J.; Maleev, A. V.; Misquitta, A. J.; Mohamed, S.; Needs, R. J.; Neumann, M. A.; Nikylov, D.; Orendt, A. M.; Pal, R.; Pantelides, C. C.; Pickard, C. J.; Price, L. S.; Price, S. L.; Scheraga, H. A.; van de Streek, J.; Thakur, T. S.; Tiwari, S.; Venuti, E.; Zhitkov, I. K. *Acta Crystallogr., Sect. B* **2011**, *67*, 535−551.

(24) Grimme, S. *J. Comput. Chem.* **2006**, *27*, 1787−1799.

(25) Grimme, S.; Antony, J.; Ehrlich, S.; Krieg, H. *J. Chem. Phys.* **2010**, *132*, 154104.

(26) Becke, A. D.; Johnson, E. R. *J. Chem. Phys.* **2005**, *122*, 154104.

(27) Johnson, E. R.; Becke, A. D. *J. Chem. Phys.* **2005**, *123*, 024101.

(28) Becke, A. D.; Johnson, E. R. *J. Chem. Phys.* **2006**, *124*, 014104.

(29) Becke, A. D.; Johnson, E. R. *J. Chem. Phys.* **2007**, *127*, 154108.

(30) Tkatchenko, A.; Scheffler, M. *Phys. Rev. Lett.* **2009**, *102*, 073005.

(31) Dion, M.; Rydberg, H.; Schröder, E.; Langreth, D. C.; Lundqvist, B. I. *Phys. Rev. Lett.* **2004**, *92*, 246401.

(32) Vydrov, O. A.; Van Voorhis, T. *J. Chem. Phys.* **2010**, *133*, 244103.

(33) Schatschneider, B.; Liang, J.; Reilly, A. M.; Marom, N.; Zhang, G. X.; Tkatchenko, A. *Phys. Rev. B* **2013**, *87*, 060104.

(34) Pedone, A.; Presti, D.; Menziani, M. C. *Chem. Phys. Lett.* **2012**, *541*, 12−15.

(35) Presti, D.; Pedone, A.; Menziani, M. C.; Civalleri, B.; Maschio, L. *CrystEngComm* **2014**, *16*, 102−109.

(36) Dovesi, R.; Saunders, V. R.; Roetti, C.; Orlando, R.; Zicovich-Wilson, C. M.; Pascale, F.; Civalleri, B.; Doll, K.; Harrison, N. M.; Bush, I. J.; D'Arco, P.; Llunell, M. *CRYSTAL09 User's Manual*; University of Torino: Torino, Italy, 2009.

(37) Dovesi, R.; Orlando, R.; Civalleri, B.; Roetti, C.; Saunders, V. R.; Zicovich-Wilson, C. M. *Z. Kristallogr.* **2005**, *220*, 571−573.

(38) Becke, A. D. *J. Chem. Phys.* **1993**, *98*, 5648−5652.

(39) Stephens, P.; Devlin, F.; Chabalowski, C.; Frisch, M. J. *J. Phys. Chem.* **1994**, *98*, 11623−11627.

(40) Civalleri, B.; Zicovich-Wilson, C. M.; Valenzano, L.; Ugliengo, P. *CrystEngComm* **2008**, *10*, 405−410.
(41) Peterson, K.; Figgen, D.; Dolg, M.; Stoll, H. *J. Chem. Phys.* **2007**, *126*, 124101.
(42) Igel-Mann, G.; Stoll, H.; Preuss, H. *Mol. Phys.* **1988**, *65*, 1321.
(43) http://www.theochem.uni-stuttgart.de/pseudopotentials/.
(44) Pickard, C.; Mauri, F. *Phys. Rev. B* **2001**, *63*, 245101.
(45) Yates, J.; Pickard, C.; Mauri, F. *Phys. Rev. B* **2007**, *76*, 024401.
(46) Segall, M. D.; Lindan, P. J. D.; Probert, M. J.; Pickard, C. J.; Hasnip, P. J.; Clark, S. J.; Payne, M. C. *J. Phys.: Condens. Matter* **2002**, *14*, 2717.
(47) Clark, S.; Segall, M.; Pickard, C.; Hasnip, P.; Probert, M.; Refson, K.; Payne, M. *Z. Kristallogr.* **2005**, *220*, 567−570.
(48) Perdew, J.; Burke, K.; Ernzerhof, M. *Phys. Rev. Lett.* **1996**, *77*, 3865−3868.
(49) Pedone, A.; Charpentier, T.; Menziani, M. C. *Phys. Chem. Chem. Phys.* **2010**, *12*, 6054−6066.
(50) De Gortari, I.; Portella, G.; Salvatella, S.; Bajaj, V. S.; van der Wel, P. C. A.; Yates, J. R.; Segall, M. D.; Pickard, C. J.; Payne, M. C.; Vendruscolo, M. *J. Am. Chem. Soc.* **2010**, *132*, 5993−6000.
(51) Dumez, J.-N.; Pickard, C. J. *J. Chem. Phys.* **2009**, *130*, 104701−104708.
(52) Barone, V.; Cimino, P.; Pedone, A. *Magn. Reson. Chem.* **2010**, *48*, S11−S22.
(53) Bader, R. F. W. *Chem. Rev.* **1991**, *130*, 893−928.
(54) Tang, W.; Sanville, E.; Henkelman, G. *J. Phys.: Condens. Matter* **2009**, *21*, 084204.
(55) Sanville, E.; Kenny, S. D.; Smith, R.; Henkelman, G. *J. Comput. Chem.* **2007**, *28*, 899−908.
(56) Henkelman, G.; Arnaldsson, A.; Jónsson, H. *Comput. Mater. Sci.* **2006**, *36*, 354−360.

dx.doi.org/10.1021/ic5006743 | *Inorg. Chem.* 2014, 53, 7926−7935